Solid-state platform for space-time engineering: The 8*Pmmn* borophene sheet

T. Farajollahpour,[1] Z. Faraei,[1] and S. A. Jafari[1,2,*]

[1]*Department of Physics, Sharif University of Technology, Tehran 11155-9161, Iran*

[2]*Center of excellence for Complex Systems and Condensed Matter (CSCM), Sharif University of Technology, Tehran 1458889694, Iran*

(Received 25 March 2019; published 26 June 2019)

We construct the most generic Hamiltonian of the 8*Pmmn* structure of a borophene sheet in the presence of spin orbit, as well as background electric and magnetic fields. In addition to spin and valley Hall effects, this structure offers a framework to conveniently manipulate the resulting "tilt" of the Dirac equation by applying appropriate electric fields. Therefore, the tilt can be made space as well as time dependent. The border separating the low-field region with undertilted Dirac fermions from the high-field region with over-tilted Dirac fermions will correspond to a black-hole horizon. In this way, space-time-dependent electric fields can be used to *design* the metric of the resulting space-time felt by electrons and holes satisfying the tilted Dirac equation. Given that the velocity of light is replaced by a two to three orders-of-magnitude smaller Fermi velocity, the tests of gravity when imported to our solid-state setting will correspond to four to six orders-of-magnitude larger effects. Our platform offers a way to generate analogues of (nonpropagating) gravitational waves by electric fields (rather than by mass sources) which can be detected in solid-state spectroscopies as enhanced superconducting correlations.

DOI: 10.1103/PhysRevB.99.235150

I. INTRODUCTION

The dynamics of elementary particles is severely restricted by imposing the symmetry of vacuum, namely, the Lorentz symmetry on them. However, elementary excitations in solid-state systems are mounted on a lattice. As such, the low-energy (long wavelength) effective electronic degrees of freedom in solid-state systems are not obliged to satisfy the Lorentz symmetry, although they might do so, as in graphene sheets [1,2] and $3+1$-dimensional Dirac materials [3,4]. There are 230 possible symmetry structures on lattices [5], some of which have nonsymmorphic symmetry elements, namely, elements that are a combination of point-group operations with fractional translation. The Bloch phase resulting from the shift can, for example, give rise to a class of fermions dubbed nexus fermions which have no counterpart in the realm of elementary particles, as they boldly contradict the famous spin-statistics theorem, according to which all fermions must have half-integer spins [6,7].

The purpose of this paper is to show that the nonsymmorphic symmetry elements have at least the following interesting geometric effect, namely, (1) *the continuum limit of the resulting tilted Dirac theory is not the Minkowski spacetime* [8] and (2) *the properties of the resulting space-time can be controlled by perpendicular electric fields*. In fact, the resulting Dirac theory on the background of such lattices is specified by two velocity scales: (i) the major velocity v_F (that replaces the light velocity of high-energy relativistic theories) and (ii) the tilt velocity v_t. The ratio between these two parameters $\eta = v_t/v_F$ determines the type of tilted Dirac cone. The situation with $0 < \eta < 1$ ($1 < \eta$) in Fig. 1 is undertilted (overtilted). Trying to tilt the Dirac equation in symmorphic structures such as graphene by applying strains will only produce very little tilt [9,10], while the pristine tilt in borophene is $\eta \sim 0.4$ [11]. This signifies the importance of the underlying nonsymmorphic lattice structure which serves to produce a substantial tilt even in the nonstrained structure. Not only that, as we will show in this paper, the peculiar symmetry of 8*Pmmn* borophene forces the background electric (and magnetic) fields to couple to electronic degrees of freedom in such a way that the tilt velocity v_t can be directly tuned by the electric field. Such a peculiar form of coupling with external electromagnetic fields can not be achieved in symmorphic lattices.

To set the stage for our work, let us start by the minimal form of tilted Dirac equation in two space dimensions, which for a single valley is given by [12–14]

$$H = \hbar v_F \begin{pmatrix} \eta k_x & k_x - ik_y \\ k_x + ik_y & \eta k_x \end{pmatrix} = \hbar v_F (\eta k_x \tau_0 + \boldsymbol{k}\cdot\boldsymbol{\tau}), \quad (1)$$

where τ_0 is the unit 2×2 matrix and $\tau_{i=1,2}$ are Pauli matrices. To make the physics transparent, we have used our freedom to choose a coordinate system such that the k_x axis is along the tilt direction. From the effective theory of 8*Pmmn* borophene, it follows that the effective Hamiltonian around the other valley is obtained by $\eta \to -\eta$ and $\tau_x \to -\tau_x$. So, the valley degrees of freedom can be labeled by $\zeta = \pm 1$ (see Appendices). The possible anisotropy of the Fermi velocity v_F [15] can be removed by a rescaling of momenta (or coordinates) which will give rise to a constant Jacobian and does not alter the physics. The dispersion relation for this tilted Dirac cone Hamiltonian is given by

$$E_s(\boldsymbol{k}) = k(s + \eta\cos\theta_{\boldsymbol{k}}), \quad (2)$$

where $s = \pm 1$ refers to positive (E_+) and negative (E_-) energy states, and $\theta_{\boldsymbol{k}}$ is polar angle of the two-dimensional wave vector, $\boldsymbol{k}$, with respect to the x axis.

*akbar.jafari@gmail.com

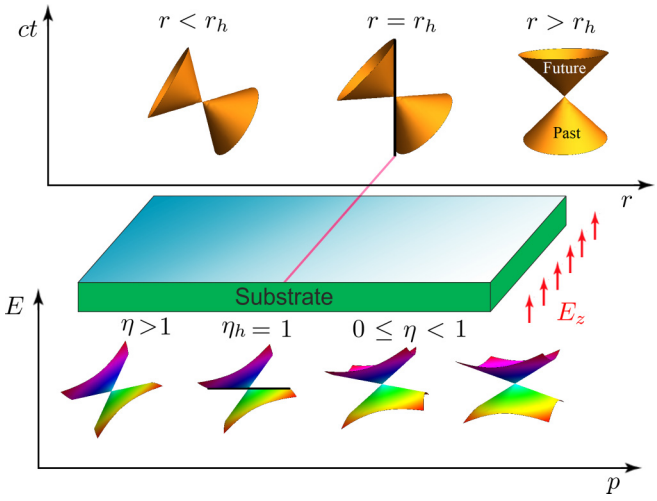

FIG. 1. Schematic illustration of the low-energy physics (solid state) analog of the black-hole horizon in 8*Pmmn* lattice. The strong-field region will correspond to the interior of the black hole.

Following Volovik [16–18], let us view the dispersion of a tilted Dirac cone as a null-surface in a Painelevé-Gullstrand (PG) space-time:

$$ds^2 = -v_F^2 dt^2 + (d\boldsymbol{r} - \boldsymbol{v}_t dt)^2. \tag{3}$$

The v_t can have arbitrary dependence on space-time coordinates. When v_t is inversely proportional to the radial coordinate, i.e., $\eta = v_t/v_F = r_h/r$ (where $r_h = 2GM/v_F$ is the solid-state horizon radius), the resulting PG metric will be a coordinate transformation of celebrated Schwartzchild space-time [19] that remains regular at the horizon [20]. In our paper, v_t can be arbitrary and we will show that it is solely controlled by the perpendicular electric field. Therefore, in 8*Pmmn* borophene, the geometry of such a generic PG space-time can be engineered via engineering the space-time profile of v_t or equivalently η. The dispersion of massless particles in this space-time is given by $g^{\mu\nu}k_\mu k_\nu = 0$ with $k_\mu = (E, \boldsymbol{k})$ or, equivalently, $(E - \boldsymbol{k}\cdot\boldsymbol{v}_t)^2 - v_F^2 k^2 = 0$, which is equivalent to the dispersion relation (2). When the tilt velocity is allowed to depend on the radial coordinate as $v_t/v_F = r_h/r$, the overtilted situation $v_t > v_F$ corresponds to $r < r_h$, which defines the black-hole in this space-time geometry as in Fig. 1. Gapping out the Dirac equation does not alter the space-time geometry as it simply corresponds to energy-momentum tensors satisfying $g_{\mu\nu}k^\mu k^\nu = m^2$ where the metric $g_{\mu\nu}$ is the same as the massless case.

Unlike existing proposals of black-hole physics [21] in condensed matter systems based on liquid helium [22] or Bose-Einstein condensates in three space dimensions [23,24], which require very low temperature or high pressures, the 8*Pmmn* borophene sheet (Fig. 2) offers a solid-state system at ambient conditions with additional tunability to explore black-hole physics on the tabletop. Recent solid-state proposals in $3+1$ dimensions employ the external strain [25] or intrinsic inhomogeneity [26] where a type-III Weyl material with $\eta = 1$ (right at the horizon) can *slightly* change to either $\eta < 1$ or $\eta > 1$ (see Fig. 1). Building on pioneering works of Volovik, authors of Ref. [25] explore the warping of space-time by uniaxial strain. They analyze the possibilities to simulate black holes and white holes, and gravitational lensinglike effects in $3+1$-dimensional Dirac semimetals. In our proposal, apart from dealing with a $2+1$-dimensional space-time which makes our system a unique space-time laboratory on the tabletop, the electric field offers a wide tunability compared to slight changes induced by strain [25]. Furthermore, being two-dimensional allows us to "pattern" the electric field to design arbitrary $2+1$-dimensional space-time. Even if patterning the electric field of an arbitrary profile poses technological challenges, a simple step-function profile of an electric field consisting of two regions of high and low fields which can be achieved by two separate capacitors would be enough for our purposes.

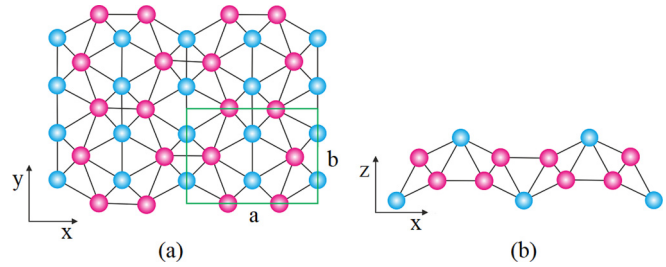

FIG. 2. Lattice structure of 8*Pmmn* borophene: (a) top view (b) side view. Green rectangle is the unit cell.

II. RESULTS AND CANDIDATE MATERIAL

As pointed out earlier, the nonsymmorphic structure of the lattice is essential to produce substantial tilt in the pristine form [27]. Boron is the light element with the atomic number $Z = 5$ which is on the left of carbon in the periodic table of elements. It has a number of structures [28], some of which are synthesized [29–34]. We will be dealing with the 8*Pmmn* structure shown in Fig. 2 which is predicted to be stable [35–38]. Earlier layered material hosting tilted Dirac cone was the α-BEDT organic conductor [15]. The common feature of 8*Pmmn* borophene, apart from hosting the tilted Dirac cones [39], is that the low-energy degrees of freedom in both systems is built from molecular orbitals [37] rather than the atomic orbitals. However, their essential difference is that the organic conductor is a layered material, while 8*Pmmn* borophene is an atom-thick two-dimensional material. In symmorphic structures such as graphene, the amount of tilt that can be extrinsically produced by applying an appropriate strain on it is negligible. Furthermore, the electric field tunability of the tilt parameter of borophene is not available in graphene. Therefore, we are left with only one suitable choice among the present three possible $2+1$-dimensional tilted Dirac cone systems.

A simple quantum chemical picture of why the 8*Pmmn* structure shown in Fig. 2 hosts tilted Dirac cone is as follows[1]: The number of blue atoms is equal to the number of red atoms. Each blue atom transfers one electron to the red atom subsystem. As these two sets of atoms are geometrically

[1]This picture is due to G. Baskaran.

inequivalent and bonded differently, electronegativity could become different, resulting in charge transfer. B^{+1} ions form one-dimensional chains, via strong sp^1 bonding within each chain. The positively charged insulating chains are alternately displaced up and down along the perpendicular direction. Red B^{-1} atoms form (silicenelike) honeycomb lattice; in addition, it is also elongated along the chain direction. Three valence electrons disappear via some kind of sp^3 bonding. We are left with one valence electron per red B atoms. Now the problem is close to the case of graphene (one valence electron per B atom) with anisotropic hopping matrix elements along and perpendicular to chain directions. This will lead to a tilted Dirac cone at K points. Amount of tilting is determined by the anisotropy. Wannier functions in the above description are primarily localized on red atoms with admixture from neighboring blue and red atoms.

Search for other $2+1$-dimensional systems with substantial intrinsic tilt deformation of the Dirac equation remains an open problem.

III. EFFECTIVE HAMILTONIAN

The most generic $8Pmmn$-invariant 4×4 Hamiltonian in the basis of molecular orbitals, $|\psi^c,\frac{1}{2}\rangle$, $|\psi^v,\frac{1}{2}\rangle$, $|\psi^c,-\frac{1}{2}\rangle$, $|\psi^v,-\frac{1}{2}\rangle$ is given by (see the Appendices for details)

$$\begin{aligned} H &= f(\vec{k})\sigma_0\tau_0 + m(\vec{k})\sigma_0\tau_3 + t_0k_x\sigma_0\tau_2 + \Delta_{\mathrm{KM}}k_y\sigma_3\tau_1 \\ &\quad + \sum_{i,j=1}^{2} k_i\sigma_j\epsilon_{ij}\left(\lambda^R_{0,i}\tau_0 + \lambda^R_{3,i}\tau_3\right) + (\lambda_2\sigma_2 + \lambda_1k_xk_y\sigma_1)\tau_2 \\ &\quad + \sum_{i=1}^{3} B_i\sigma_i g_{0,i}\tau_0 + M_i^{\mathrm{int}}g_{3,i}\tau_3, \end{aligned} \tag{4}$$

where $f(\vec{k}) = f_0 + f_1k_x^2 + f_2k_y^2$, $m(\vec{k}) = m_1k_x^2 + m_2k_y^2 - m_0$ and we have used the explicit form of Γ matrices in terms of the direct product of Pauli matrices σ (in spin-space) and τ (in molecular orbital space). Δ_{KM} is spin-orbit coupling of the Kane-Mele type [40], $\lambda^R_{0,i}$ and $\lambda^R_{3,i}$ for $i=1,2$ are anisotropic Rashba spin-orbit coupling. $\lambda^R_{0,i}$ is proportional to external electric field [41] while $\lambda^R_{3,i}$ is similar to "buckling" term of silicene structure [28]. λ_1,λ_2 are forms of spin-orbit coupling which are specific to the $8Pmmn$ structure. The λ couplings are proportional to the coordinate z itself. Similarly, in the last line, we have two types of Zeeman coupling. The terms containing τ_0 are related to coupling to external field B, and the term containing τ_3 is due to internal exchange fields which roots in the orbital angular momentum of the molecular orbitals involved. In both electric- and magnetic-field-related terms, those couplings carrying the subscript 3 which are coupled to τ_3 arise from internal fields specific to $8Pmmn$ structure. The lack of symmetry under $z\to -z$ prevents them from vanishing.

A. Spin Hall effect in borophene

The first line of Eq. (4) is what gives the long-wavelength limit in Eq. (1). As long as only the first line is concerned, a pair of tilted Dirac cones at $\vec{k}^\zeta = (0,\zeta k_D)$ along the ΓY line are obtained, where $k_D = \sqrt{m_0/m_2}$ and $\zeta = \pm$ is the valley index. The tilt is then controlled by f_2 parameter. The second line is related to spin-orbit coupling. Generically, this term generates a gap in the tilted Dirac cone spectrum. The reason is simple, because in the first line τ_3 and τ_2 are already used, and the second line containing τ_1 in two space dimensions will always generate a gap. To see this, let us define $\vec{p} = \vec{k} - \vec{k}^\zeta$ and linearize the above Hamiltonian when only the first two lines are present:

$$H = F_0\tau_0 + F_1\sigma_3\tau_1 + F_2\tau_2 + F_3\tau_3, \tag{5}$$

where $F_0 = 2\zeta f_2k_Dp_y$, $F_1 = \zeta\Delta_{\mathrm{KM}}k_D + \Delta_{\mathrm{KM}}p_y$, $F_2 = t_0p_x$ and $F_3 = 2\zeta m_2k_Dp_y$. The spectrum of the above Hamiltonian for two eigenvalues $\sigma_3 = \pm 1$ (corresponding to $\uparrow$ and $\downarrow$ states) is given by

$$2\zeta f_2k_Dp_y \pm \sqrt{\Delta^2_{\mathrm{KM}}(\zeta k_D + p_y)^2 + (t_0p_x)^2 + 4(m_2k_Dp_y\sigma_3)^2}.$$

As can be seen, the tilt is controlled by ζf_2k_D and is therefore opposite for the two valleys. Moreover, at Dirac nodes $\vec{k}^\zeta$, we have $\vec{p}=0$ and therefore the resulting mass term is a *Haldane mass* and will be given by $\zeta\Delta_{\mathrm{KM}}k_D$ [42] which will give rise to spin Hall effect (SHE) [43–45]. Hydrogenation brings in some sp^3 component which enhances the spin-orbit term (Δ_{KM} in our case). The valley and spin dependence of the gap lies at the core of a proposal by Kane and Mele [40]. Observation of this effect for hydrogenated graphene has been discussed by Balakrishnan *et al.* [46]. The further control parameter in the case of borophene is that in addition to the extrinsic enhancement of spin-orbit coupling (Δ_{KM}), one can also use the strain to manipulate k_D [47,48].

A very important property of borophene in contrast to graphene is that, while in graphene both topologically trivial Dirac mass and topologically nontrivial Haldane mass are allowed by symmetries of the lattice, in the case of borophene, as long as it remains in the $8Pmmn$ symmetry group, the Haldane mass is the *only* possible form of gap. To see this, let us try to add a gap-opening term proportional to τ_1. If it is not of the $\sigma_3\tau_1$ form, then it must be proportional to $\sigma_0\tau_1 = \Gamma_{45}$, which belongs to B_{3u} representation (see Appendices) and is even with respect to time reversal. But the basis functions in this representation are odd with respect to time reversal (TR). This means that *only spin-orbit coupling is able to gap out the tilted Dirac cone spectrum of* $8Pmmn$ *borophene.* Indeed, this has been confirmed by *ab initio* calculations. In the case of pristine borophene where only intrinsic spin-orbit coupling exists, the spin-orbit-induced gap is $\sim$0.03 meV, while for hydrogenated borophene the buckling arising from sp^3 nature of the bonds will give extrinsic contribution to spin-orbit coupling [49] which then generates two orders-of-magnitude larger spin-orbit gap $\sim$2.25 meV [11]. Note that, although the gap opening comes from σ_3 term, the two spin subbands corresponding to $\uparrow$ and $\downarrow$ spins remain degenerate as $\sigma_3^2 = (\pm 1)^2 = +1$. The effect of spin-orbit coupling in $8Pmmn$ group is different from, e.g., $P4/nmm$ group where even spin-orbit coupling is not able to gap out the resulting two-dimensional Dirac cone [50].

A further prediction of the first two lines of our effective Hamiltonian Eq. (4) which may be relevant to 8*Pmmn* crystals other than borophene is that if a material in this group happens to have $m_0 = 0$, we will have $k_D = 0$ and therefore the Dirac cone will move to Γ pint. This will have two consequences: (i) The gap which is controlled by Haldane mass $\zeta \Delta_{\rm KM} k_D$ vanishes. (ii) The tilt which is controlled by the $\zeta f_2 k_D$ combination also vanishes. Therefore, as $m_0 \to 0$, the two tilted gapped Dirac spectrums with opposite tilt move toward each other and collide at Γ pint, whereby both gap and tilt are destroyed. Since the $\Delta_{\rm KM}$ term being related to spin-orbit coupling is nonzero for extrinsic or intrinsic reasons, the only way to diminish the Haldane mass will be to require $k_D = 0$. But this will also diminish the tilt. In this way, the SHE and tilt are locked to each other and always go hand in hand. This suggests a possible connection between the tilt and the Z_2 index of the resulting SHE state.

B. Electric field effects

Now let us discuss the third and fourth line of our effective Hamiltonian, Eq. (4). The spin structure is of the Rashba form $\boldsymbol{k} \times \vec{\sigma}.\vec{z}$, where $\vec{z} = z\hat{z}$ is a vector perpendicular to the crystal sheet. This term being proportional to the real space coordinate z is related to a linear electrostatic profile which is equivalent to a constant electric field, E_z perpendicular to the borophene sheet. Having a Rashba spin-orbit coupling form can be potentially useful in spintronic applications [45]. The origin of the electric field can be extrinsic or intrinsic. The externally applied electric field couples to both conduction and valence states on equal footing. Therefore, it will be isotropic in τ space and hence will be coupled through τ_0. This accounts for the first term in the third line where Rashba parameters $\lambda^R_{0,i}$ are introduced and they are related to external electric field by $E_{\rm ext} z \alpha_i = \lambda^R_{0,i}$, where α_i with $i = 1, 2$ accounts for the anisotropy of the crystal. In the isotropic approximation, this constant will not depend on the direction i. The second term $\lambda^R_{3,i}$ is coupled via τ_3, meaning that it couples asymmetrically to molecular orbital degrees of freedom forming the conduction and valence bands. This can be traced back to the lack of symmetry under $z \to -z$ of the crystal in Fig. 2 which gives rise to staggered polarization pattern.

This staggered polarization when projected in the space of low-energy molecular orbitals $|\psi^c\rangle$ and $|\psi^v\rangle$, generates τ_3 term as in the third line of Eq. (4). Similar arguments apply to the fourth line. Therefore, couplings $\lambda^R_{3,i}$, λ_2, and λ_1 arise from internal polarization fields and are fixed by materials parameters. Progress in the calculation of polarization for periodic solids [51,52] can be employed to obtain *ab initio* estimates of these couplings for 8*Pmmn* borophene.

The matrix structure of the third line in the space of molecular orbitals is $\lambda^R_{0,i}\tau_0 + \lambda^R_{3,i}\tau_3 = {\rm diag}(\lambda^R_{0,i} + \lambda^R_{3,i}, \lambda^R_{0,i} - \lambda^R_{3,i})$. Since λ^R_0 can be externally tuned by applied electric field, it can be used to tune either of the upper or lower diagonal components to zero. In this way, the the resulting (anisotropic) Rashba term will become orbital selective [53]. A uniaxial strain is expected to distort the low-energy molecular orbitals whereby the intrinsic $\lambda^R_{3,i}$ couplings can be changed [47,48].

C. Tunable tilt: A tool for space-time engineering

Now we are ready to discuss the most important message of our work, which is the tuning of the tilt parameter by electric fields in 8*Pmmn* borophene sheets. The role of all λ terms in Eq. (4) is to generate spin-orbit gaps (see the next subsection). But since boron is a very light element, the intrinsic spin-orbit gaps are on the scale of 0.02 meV [11]. Therefore, we can ignore the mass terms. To look into the velocity scales in x direction, we set $p_y = 0$ in Eq. (9) to obtain

$$\begin{aligned} \varepsilon_\tau(p_x) &= s p_x \sqrt{t_0^2 + u^2 + 2\tau w^2}, \\ u^2 &= \lambda_1^2 k_D^2 + \left(\lambda^R_{3,1}\right)^2 + \left(\lambda^R_{0,1}\right)^2, \\ w^4 &= \lambda_1^2 k_D^2 \left(\lambda^R_{3,1}\right)^2 + t_0^2\left[\left(\lambda^R_{0,1}\right)^2 + \left(\lambda^R_{3,1}\right)^2\right], \end{aligned} \tag{6}$$

where $s = \pm 1$ are eigenvalues of σ_3 and $\tau = \pm 1$ refer to the eigenvalues of τ_3 matrix. Now define the tilt and major velocity scale by $v_t = \frac{v_+ + v_-}{2}$, $v_F = \frac{v_+ - v_-}{2}$, where $v_\pm$ correspond to $\tau = \pm 1$ in the above dispersion. Then in the limit of very large electric fields such that $\lambda^R_{0,1} \gg t_0$, we obtain

$$v_{tx} \approx \left(t_0^2 + u^2\right)^{1/2}, \quad v_{Fx} \approx \frac{w^2}{\sqrt{t_0^2 + u^2}}. \tag{7}$$

In this limit, the major Fermi velocity v_{Fx} is saturated, while, remarkably v_{tx} is linearly controlled by the electric field. Similarly, to investigate the velocity scales related to y direction, we ignore the gap and set $p_x = 0$ which gives

$$v_{ty} = 2\zeta f_2 k_D + s\lambda^R_{0,2}, \quad v_{Fy} = 2\zeta m_2 k_D + s\lambda^R_{3,2}. \tag{8}$$

This again shows a linear dependence of the v_{ty} to electric field, while the v_{Fy} does not change by electric field.

Therefore, the major Fermi velocities v_{Fi} determining the solid angle subtended by the Dirac cone are essentially controlled by intrinsic parameters and intrinsic (albeit anisotropic) Rashba couplings $\lambda^R_{3,i}$, while the corresponding tilt velocity v_{ti} is controlled by external electric field $\lambda^R_{0,i}$. The intrinsic Rashba spin-orbit energy scales for pristine borophene are $\lambda^R_{3,i} \sim 10^{-2}$ meV. By hydrogenation and introducing sp^3 component, it can be enhanced up to ∼2 meV [11]. At energy scales well above these scales, the spin-orbit gap can be ignored, and we are essentially dealing with a gapless (two-space dimensional) Dirac node. When the external electric field is zero, the cone is given by the tilt parameter $\eta = 3.4/8.0 \sim 0.4$ [11]. By increasing the external electric field, this value will keep increasing. Beyond the point corresponding to $\eta_h = 1$, it will be overtilted [16,17]. The reason we have used the subscript h (for horizon) rather than c (for critical) is to emphasize gravitational analogy [16,17,22].

Therefore, 8*Pmmn* borophene is a promising solid-state platform where a background electric field can manipulate the tilt velocity scales. Although the the tuning of the tilt within the current experimental conditions appears to be challenging [11], the ability to tune the tilt of a Dirac cone is already interesting by itself. Larger tilt enhances the effect of Landau quantizations and makes the ultra quantum limit much more accessible than the upright Dirac cone [12]. Also, when it comes to plasmon oscillations, the tilt gives rise to a kink in the plasmon spectrum [13,14]. An interesting amplification of

magnetic fields by crossed electric fields can also be achieved in tilted Dirac cone systems where the effective "tilt-boosted" magnetic fields felt in the two valleys are reciprocally related [8].

Equipped with the gravitational analogy, 8*Pmmn* borophene can be viewed as a "black hole on the tabletop" [2]: One can apply strong enough perpendicular electric field to a portion of borophene sample. The region with the strong field will correspond to overtilted Dirac cone, while the low-field region will be described by undertilted Dirac equation. The strong-field region will correspond to the interior of the black hole, while the low-field region will correspond to the exterior of the black hole as in Fig. 1. Moving across the horizon in Fig. 1 corresponds to the Lifshitz transition of the Dirac dispersion which will leave a signature in superconducting correlations [54]. Letting the electric field profile oscillate with time will force the horizon to oscillate. This will act like a source of "gravitational" waves in the sense that it corresponds to the oscillatory behavior of the metric. But since in $2+1$ dimensions, there are no degrees of freedom left to form propagating gravitational modes, it can only be sustained in the form of forced oscillations. Note that in Einstein equation, the "source" determining the metric is the mass content of space-time, while in our case the metric is determined by background electric field. Scanning the borophene surface with a scanning tunneling microscope (STM) can detect that oscillations of the metric in the form of oscillatory superconducting correlations. Any time the STM tip reaches a distortion of space-time in the form of a "tilt-hump" with $\eta \approx 1$, it will detect an enhancement of superconducting correlations [54]. Therefore, the condensed matter analog of (nonpropagating) "gravitational waves" in our simulated space-time are oscillations of superconducting correlations.

Another effect of the horizon in condensed matter applications would be that the electron-hole pairs created by, e.g., sun light near the horizon will have some chance to enter the black hole. Even a small in-plane electric field bias can encourage, e.g., holes more than electrons to dive into a black hole where their future light cone limits them to $\eta > 1$ region. Therefore, the horizon is a barrier for the recombination of electron-hole pairs. Given the two space dimensional nature of our system, this effect may find potential applications in solar cells where reduction of electron-hole recombination is a merit.

D. Valley Hall effect

Now let us discuss the physics of λ terms which are Rashba type and 8*Pmmn* generalizations of Rashba. Typical scale of λ_0^R terms arising from electric fields in Germanene is $\sim$10 meV [55] while in the intrinsic case $\Delta_{\rm KM} \sim 0.03$ meV [11]. Therefore, let us ignore the Kane-Mele term, and focus on the λ-terms only. The essential role of λ terms is to open spin-orbit gaps, whereby to generate Dirac mass for the fermions of Eq. (1). The effective Hamiltonian around the Dirac valley labeled by $\zeta = \pm 1$ is given by ($\Delta_{\rm KM} = 0, B = 0$)

$$H = \left(F_0 + \lambda_{0,1}^R p_x\sigma_2 - \lambda_{0,2}^R p_y\sigma_1 - \zeta\lambda_{0,2}^R k_D\sigma_1\right)\tau_0$$

[2]In the same spirit that graphene is thought of as CERN on the tabletop.

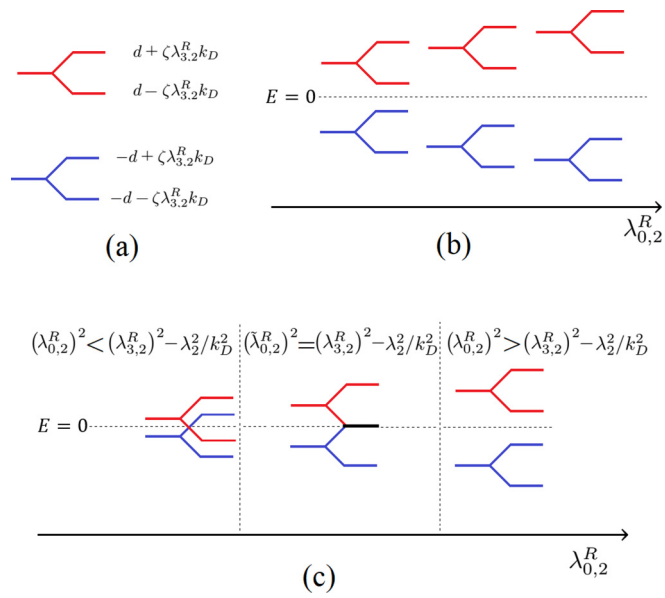

FIG. 3. Schematic level diagram in the presence of external electric field. $\zeta = \pm 1$ labels the two valleys. d is defined in Eq. (11). (a) is a generic level diagram. (b) shows the schematic behavior of the band edges as a function of $\lambda_{0,2}^R$. (c) change of band edge arrangements from weak (left) to strong fields (right).

$$+ (F_2 + \zeta\lambda_1 k_D p_x\sigma_1 + \lambda_2\sigma_2)\tau_2$$
$$+ \left(F_3 + \lambda_{3,1}^R p_x\sigma_2 - \lambda_{3,2}^R p_y\sigma_1 - \zeta\lambda_{3,2}^R k_D\sigma_1\right)\tau_3, \quad (9)$$

where F_μ coefficients are given below Eq. (5). Setting $p_x = p_y = 0$, we obtain the "gap matrix" as

$$g = -\zeta\lambda_{0,2}^R k_D\sigma_1\tau_0 + \lambda_2\sigma_2\tau_2 + \zeta\lambda_{3,2}^R k_D\sigma_1\tau_3. \quad (10)$$

Note that the only $\lambda_{0,2}^R$ and $\lambda_{3,2}^R$ appear in the gap matrix. The other two Rashba terms corresponding to x direction, namely, $\lambda_{0,1}^R$ and $\lambda_{3,1}^R$, appear as coefficients of p_x term. Their role is to renormalize the Fermi velocity and the velocity scale associated with the tilt which was discussed in previous next subsection. Corresponding to two eigenvalues $s = \pm 1$ of matrix σ_3, the eigenvalues of the above matrix are

$$-d \pm \zeta\lambda_{3,2}^R k_D, \quad +d \pm \zeta\lambda_{3,2}^R k_D, \quad d = \sqrt{\lambda_2^2 + \left(\zeta\lambda_{0,2}^R k_D\right)^2}. \quad (11)$$

Now there are two situations: (i) $|\lambda_2| > |\lambda_{3,2}^R| k_D$ and (ii) $|\lambda_2| < |\lambda_{3,2}^R| k_D$. These are schematically shown in Fig. 3. As can be seen from the schematic-level diagram, the spectral gap in case (i) is given by $2(d - \zeta\lambda_{3,2}^R k_D)$ [see Fig. 3(b)]. The valley symmetry is explicitly broken, which in turn will give rise to valley Hall effect. As can be seen by turning on the external field $\lambda_{0,2}^R$ and increasing it, the gap always increases, and the valley asymmetry becomes less important. Therefore, in case (i), the valley Hall effect is decreased by turning on perpendicular electric field and increasing it. Case (ii) is more interesting. In this case, the gap will be given by $-2(d - \zeta\lambda_{3,2}^R k_D)$. This quantity is positive when the external electric field is absent. At a critical value of $(\tilde{\lambda}_{0,2}^R)^2 = (\lambda_{3,2}^R)^2 - \lambda_2^2/k_D^2$, this gap vanishes, and beyond this point, the gap changes sign [see Fig. 3(c)]. In either case,

the valley Hall effect arising from the asymmetry between the Rashba gaps in the two valleys is present. But now, by increasing the externally applied perpendicular electric field, the sign of valley Hall effect can be changed.

E. Magnetic-field effects

The last line contains the effect of Zeeman coupling. In Table II of the Appendices, we have assumed that the "world" is composed of 8*Pmmn* crystal and the apparatus generating the $\vec{B}$. In this way, under time reversal, $\vec{B}$ changes sign, and therefore, to construct TR invariant Hamiltonian for the "world" (which is equivalent to breaking TR of the "system") it has to couple to appropriate Γ matrices which are odd with respect to TR. In this way, we have obtained the last line of Eq. (4). The first term of the last line is similar to the standard Zeeman coupling which couples evenly to the molecular orbital degrees of freedom ($\propto\tau_0$). However, the second term, which contains τ_3, asymmetrically couples to orbital degrees of freedom. Similar to the electric field case, the $g_{0,i}$ couplings are related to the externally applied field (or exchange field) while $g_{3,i}$ couplings are intrinsic and arise from the orbital angular momenta of the molecular orbitals involved. When the couplings are tuned to satisfy $g_{0,i} = \pm g_{3,i}$, the Zeeman coupling will be orbital selective.

To understand the physics of this line, let us assume that $\Delta_{\mathrm{KM}} \approx 0$ and $B \neq 0$,

$$H = \left(F_0 + \sum_{i=1}^{3} B_i \sigma_i g_{0,i}\right)\tau_0 + F_2\tau_2 + \left(F_3 + \sum_{i=1}^{3} M_i^{\mathrm{int}} \sigma_i g_{3,i}\right)\tau_3.$$

The magnetic field has no effect on the Fermi and tilt velocities, as there is no term related to B or M in coefficients of p_x and p_y in the Hamiltonian. The Zeeman terms generates gaps as

$$\varepsilon_g = s\sqrt{\left(B_i + \tau M_i^{\mathrm{int}}\right)^2}. \tag{12}$$

These gaps arising from magnetic field interplay with the Kane-Mele gap and will enrich the phase diagram [55].

IV. DISCUSSION AND CONCLUSIONS

We have obtained effective Hamiltonian of the nonsymmorphic 8*Pmmn* borophene sheet, which has a substantial intrinsic tilt in the spectrum of its Dirac fermions. Due to the nonsymmorphic nature of the underlying lattice, a perpendicular electric field couples to the system in such a way that it can tune the tilt parameter $v_t = \eta v_F$. The tilt parameter η, on the other hand, can be regarded as a parameter in the effective space-time felt by the electrons and holes of the 8*Pmmn* borophene (Fig. 1). The gap opening from spin-orbit coupling does not alter the geometry as the dispersion relation for massive particles will be given by $g_{\mu\nu}k^\mu k^\nu = m^2$ where $g_{\mu\nu}$ is the same metric that specifies the dispersion of massless particles. In this analogy, the border between the high field region with overtilted Dirac cone and a low-field region with undertilted Dirac cone will correspond to a horizon. Strictly speaking, the black holes as solutions of $2+1$-dimensional Einstein equation can only exist if the space-time has some sort of singularity. In a solid-state setting, this can be achieved by simply pressing an STM tip on a suspended borophene, which in the infrared looks like a conic singularity. This stabilizes the so-called BTZ black-hole [56] solution. For an electron moving near the horizon, the particle content of the states will be different from the one which is away from the horizon. Those approaching the horizon will feel more particle fluctuations which correspond to enhanced superconducting correlations in a superconducting proximity setup.

Letting the electric fields control the tilt η to oscillate will act like a source of "gravitational" waves which are albeit nonpropagating in $2+1$ dimensions as there are no degrees of freedom left in the metric as propagating modes. Such forced oscillations, however, translate into oscillations of superconducting correlations. As such, they can be detected as enhanced superconducting correlations in solid-state spectroscopies.

The ability to engineer the metric felt by electrons promotes our borophene system as a space-time simulator, albeit in $2+1$ dimensions. Given that our real world is $3+1$-dimensional, our proposal offers a unique solid-state platform to explore $2+1$ dimensional space-time which cannot be found in cosmos. Furthermore, a solid-state simulation of space-time geometry has the advantage that the velocity of the light in solid-state setting is replaced by the Fermi velocity which is two to three orders of magnitude smaller than the the speed of light. As such, tests such as Lens-Thirring precession [57] of spins will be four to six orders of magnitude larger than the corresponding precision in a true gravitational setting. This may not serve as a test of gravity, but does serve as a test of how the space-time metric and geometry [58] affects the spinning bodies.

We also discussed valley Hall effect arising from the asymmetry $\eta \to -\eta$ of the two tilts. Extrinsically enhancing the spin-orbit coupling by, e.g., hydrogenation will generate spin Hall effect which would be perhaps comparable to the same effect in hydrogenated graphene [59].

ACKNOWLEDGMENTS

We wish to thank M. Torabian, S. Baghram, M. Kargarian, M. Allaei, and A. Vaezi for fruitful discussions. T.F. appreciates Iman Ahmadabadi for useful discussion about the EBR. T.F. appreciates the financial support from Iran National Science Foundation (INSF) under postdoctoral Project No. 96015597. Z.F. was supported by Iran Science Elites Federation (ISEF) postdoctoral fellowship. S.A.J. appreciates research deputy of Sharif University of Technology, Grant No. G960214.

APPENDIX A: THE NONSYMMORPHIC 8*Pmmn* GROUP

To be self-contained, in this Appendix we present details of the 8*Pmmn* group and its representations. The lattice structure of borophene is shown in Fig. 4. The symmetry group of Borophene is 8*Pmmn*, where 8 stands for the number of atoms in the unit cell. The 8*Pmmn* is point group number 59 [60]. The generators (minimal set of elements from which all other members of the group can be constructed) are given by [5,60] $\tilde{C}_{2x} = \{C_{2x}|\frac{a}{2}00\}$, $\tilde{C}_{2y} = \{C_{2y}|0\frac{b}{2}0\}$, $\tilde{I} = \{I|000\}$, where the notation $\{C_{2x}|\mathbf{t}\}$ is a nonsymmorphic element meaning the

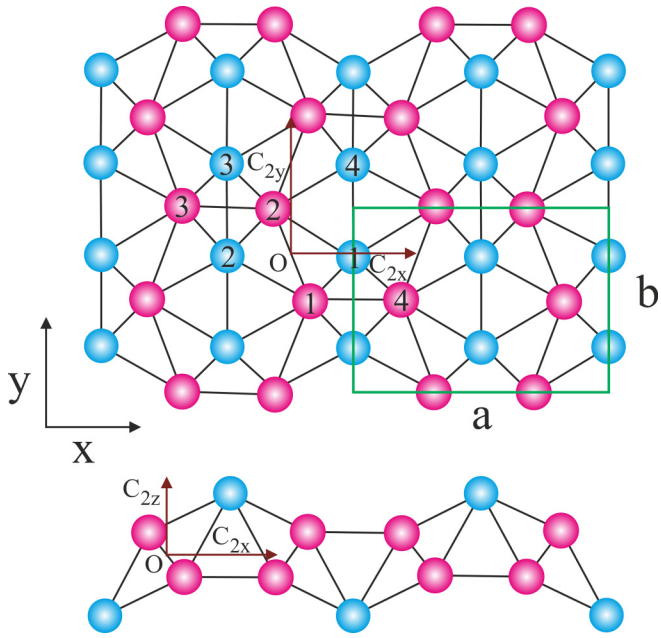

FIG. 4. Borophene lattice structure (a) top view (b) side view. The screw symmetry axes for $c\tilde{2}_x$, $c\tilde{2}_y$, and $c\tilde{2}_z$ indicated by brown. Green rectangular is the selected unit cell.

twofold rotation C_{2x} around the x axis is followed by a translation $\mathbf{t}$. All other symmetry operations of the 8*Pmmn* group can be constructed from the above generators as follows: $\tilde{C}_{2z} = \tilde{C}_{2x}\tilde{C}_{2y} = \{C_{2z}|\frac{a}{2}\frac{b}{2}0\}$, $\tilde{M}_z = \tilde{I}\tilde{C}_{2z} = \{M_z|\frac{a}{2}\frac{b}{2}0\}$, $\tilde{M}_x = \tilde{I}\tilde{C}_{2x} = \{M_x|\frac{a}{2}00\}$, and $\tilde{M}_y = \tilde{I}\tilde{C}_{2y} = \{M_y|0\frac{b}{2}0\}$ [60]. This group has eight commuting elements and therefore being Abelian, admits eight one-dimensional irreducible representations [61] given in Table I. Extensions beyond the double lines are related to the double group which is obtained by taking the spin of the electrons into account and that, upon a 2π rotation, the spinor goes into its negative [5]. The double group admits two-dimensional representations which are not relevant to our minimal 4×4 matrix representations of the effective Hamiltonian of borophene.

Nonsymmorphic elements such as "glide planes and screw axes cause the bands to *stick together* on the special surface lines and planes" [62]. Following Kittel [62], let us see how it works for the 8*Pmmn* group. In the Brillouin zone (BZ) of the

TABLE I. Character table of 8*pmmn* double group.

	E	$\tilde{c}_{2z}$	$\tilde{c}_{2y}$	$\tilde{c}_{2x}$	$\tilde{I}$	$\tilde{M}_z$	$\tilde{M}_y$	$\tilde{M}_x$	CE	$C\tilde{I}$
A_g	1	1	1	1	1	1	1	1	1	1
A_u	1	1	1	1	−1	−1	−1	−1	1	−1
B_{1g}	1	1	−1	−1	1	1	−1	−1	1	1
B_{1u}	1	1	−1	−1	−1	−1	1	1	1	−1
B_{2g}	1	−1	1	−1	1	−1	1	−1	1	1
B_{2u}	1	−1	1	−1	−1	1	−1	1	1	−1
B_{3g}	1	−1	−1	1	1	−1	−1	1	1	1
B_{3u}	1	−1	−1	1	−1	1	1	−1	1	−1
$E_{g/2}$	2	0	0	0	2	0	0	0	−2	−2
$E_{u/2}$	2	0	0	0	−2	0	0	0	−2	2

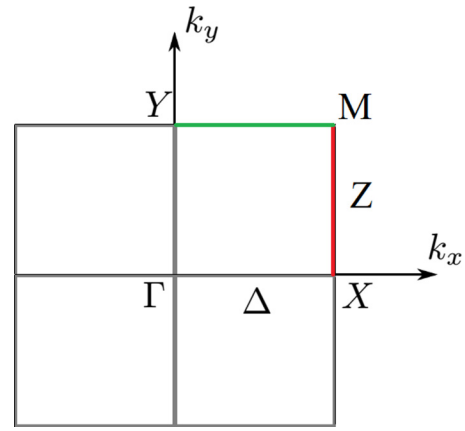

FIG. 5. Rectangular first Brillouin zone.

system (Fig. 5), let $\psi(x, y)$ be some basis wave function on the boundary line Z of the Brillouin zone (BZ). Then the screw rotation operation $\tilde{C}_{2x}$ acts as $\tilde{C}_{2x}\psi(x, y) = \psi(x + \frac{a}{2}, -y)$ while the inversion $\tilde{I}$ is defined by the operation $\tilde{I}\psi(x, y) = \psi(-x, -y)$. On other hand, $\tilde{M}_x$ acts as $\tilde{M}_x\psi(x, y) = \psi(-x + \frac{a}{2}, y)$ which means

$$\tilde{C}_{2x}\psi(x, y) = \tilde{M}_x\tilde{I}\psi(x, y). \tag{A1}$$

Now the argument by Kittel works by showing that assumption of nondegeneracy on Z line leads to contradiction [62]. So let us assume that on the Z line, the representation is one-dimensional. From $\tilde{I}^2\psi(x, y) = \psi(x, y)$, it follows that $\tilde{I}\psi(x, y) = \pm\psi(x, y)$. The same story holds for $\tilde{M}_x\psi(x, y) = \pm\psi(x, y)$. Therefore, by Eq. (A1) we must have

$$\begin{aligned}\tilde{C}_{2x}^2\psi(x, y) &= \tilde{M}_x\tilde{I}\tilde{M}_x\tilde{I}\psi(x, y) \\ &= (\pm 1)^2(\pm 1)^2\psi(x, y) = \psi(x, y).\end{aligned} \tag{A2}$$

However, from the very definition of $\tilde{C}_{2x}$ we have

$$\begin{aligned}\tilde{C}_{2x}^2\psi(x, y) &= \tilde{C}_{2x}\psi\left(x + \frac{a}{2}, -y\right) = \psi(x + a, +y) \\ &= e^{ik_x a}\psi(x, y) = e^{i\pi}\psi(x, y) = -\psi(x, y),\end{aligned} \tag{A3}$$

which contradicts Eq. (A2). Note that in the the second line we have used the Bloch theorem and that on Z line we have $k_x a = \pi$. Therefore, along the $XM = Z$ line of Fig. 5, the irreducible representations cannot be one-dimensional. Now assuming that one of the states is ψ, again a similar argument by Kittel[3] shows that both ψ and $\tilde{C}_{2x}T\psi$, where T is the time-reversal operator, are degenerate. The same considerations apply to the YM line.

Elementary band representation

In this section, by considering the Brillouin zone of the system, we obtain all the ways that are possible for energy bands to be connected to obtain realizable band structure [64–66]. In the band theory, the symmetry-enforced semimetal is realized

[3]See pages 214-215 of Kittel [62].

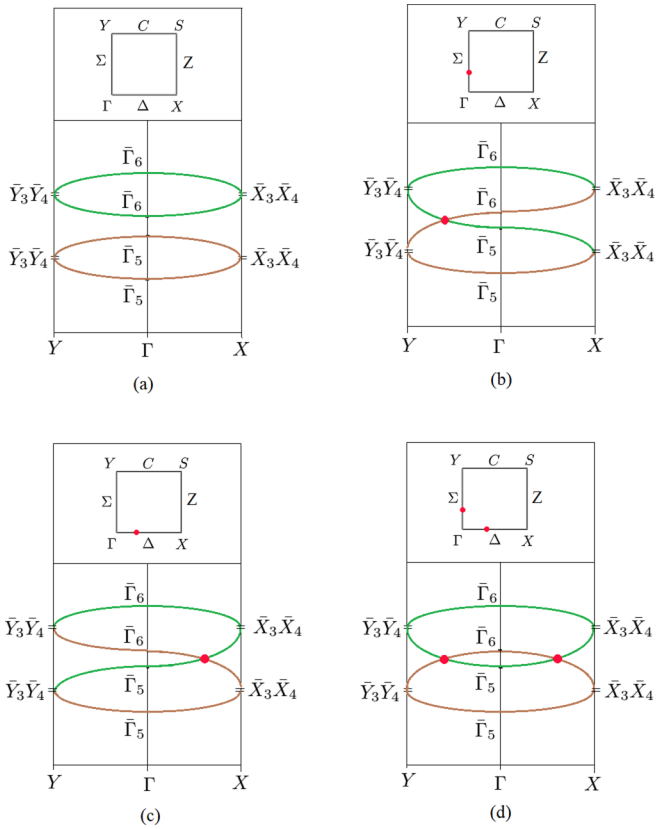

FIG. 6. Possible decomposition of elementary band representation in the presence of time-reversal symmetry labeled according to notations of Bilbao crystallography server [63]. (a) The disconnected components of EBR correspond to the insulating phase of 8*Pmmn* group materials, (b) a Dirac node points along the Γ*Y* path, (c) a Dirac node along the Γ*X* path, and (d) a pair of Dirac points along the *YΓX* path in BZ.

when the number of electrons is a fraction of the number of connections that forms an elementary band representation (EBR). The possible candidate for semimetallic materials are identified from EBRs [64–66].

The possible decomposition of EBR of the 8*Pmmn* group with time-reversal symmetry is illustrated in Fig. 6. As shown in Fig. 6(a), the disconnected components of EBR correspond to the insulating phase of 8*Pmmn* group materials. Figures 6(b) and 6(c) show a graph with connected EBR which indicate the screw-symmetry and time reversal protected topological semimetal. In these two figures [Figs. 6(b) and 6(c) Dirac nodes along the Γ*X* and Γ*Y* are obtained. According to EBR, there is yet another possibility shown in Fig. 6(d) which corresponds to two pairs of Dirac points along the *YΓX* path in BZ. However, as will become clear in the following sections and in agreement with *ab initio* calculations related to "borophene" [37], the most general Hamiltonian constructed from irreducible representations will correspond to Fig. 6(b). There can be other possible materials with the same 8*Pmmn* structure which may realize three other possibilities in Fig. 6.

APPENDIX B: MOLECULAR ORBITALS AND EFFECTIVE HAMILTONIAN

The first known example of tilted Dirac cone material is the organic conductor α-$(\mathrm{BEDT}-\mathrm{TTF})_2\mathrm{I}_3$, which is composed of molecular orbitals [15]. It was noted by Zhou *et al.* that in the case of borophene the charge density for the states at the bottom of the conduction band and top of valence band are enhanced on some bonds [37]. On the other hand, the *ab initio* calculation of Ref. [11] shows that the eigenvalues of operators $(\tilde{C}_{2x}, \tilde{C}_{2y}, \tilde{I})$ for bottom of conduction and top of valence band states are $(+1, +1, +1)$ and $(+1, -1, -1)$, respectively. This information is sufficient to let us construct most general molecular orbital consistent with the above eigenvalues. To do this, let us start from Fig. 4. The pink atoms correspond to "inner" (I) and blue atoms correspond to "ridge" (R) borons [38]. Both type of atoms are labeled by 1,2,3,4. As can be seen in Fig. 4, at the level of point group, we have following actions for the generators of 8*Pmmn* group: $\tilde{C}_{2x}$ replace $(1^{\mathrm{I}} \leftrightarrow 3^{\mathrm{I}}, 2^{\mathrm{I}} \leftrightarrow 4^{\mathrm{I}})$, $(1^{\mathrm{R}} \leftrightarrow 2^{\mathrm{R}}, 3^{\mathrm{R}} \leftrightarrow 4^{\mathrm{R}})$. For $\tilde{C}_{2y}$, we have $(1^{\mathrm{I}} \leftrightarrow 2^{\mathrm{I}}, 3^{\mathrm{I}} \leftrightarrow 4^{\mathrm{I}})$ and $(1^{\mathrm{R}} \leftrightarrow 3^{\mathrm{R}}, 2^{\mathrm{R}} \leftrightarrow 4^{\mathrm{R}})$. Finally, $\tilde{I}$ acts as $(1^{\mathrm{I}} \leftrightarrow 2^{\mathrm{I}}, 3^{\mathrm{I}} \leftrightarrow 4^{\mathrm{I}})$ and $(1^{\mathrm{R}} \leftrightarrow 2^{\mathrm{R}}, 3^{\mathrm{R}} \leftrightarrow 4^{\mathrm{R}})$. At the next level, depending on whether the relevant orbital in each of the above positions is p_x, p_y or p_z, we have

$$\tilde{C}_{2x}\{p_x\} = p_x, \tilde{C}_{2x}\{p_{y,z}\} = -p_{y,z},$$
$$\tilde{C}_{2y}\{p_y\} = p_y, \tilde{C}_{2x}\{p_{x,z}\} = -p_{x,z},$$
$$\tilde{I}\{p_{x,y,z}\} = -p_{x,y,z}.$$

It should be noted that the inversion center is located at the crossing point of two screw axes as plotted in Fig. 4. Imposing the eigenvalues $(+1, +1, +1)$ and $(+1, -1, -1)$ for the conduction and valence states, we obtain the most general molecular orbitals composing the bottom of conduction band $(|\Psi^c\rangle)$ and those at the top of valence band $(|\Psi^v\rangle)$ as follows:

$$\begin{aligned}\left|\Psi^c_{\mathrm{mol}}\right\rangle \propto\ & \alpha\left(p_x^{\mathrm{I}1} - p_x^{\mathrm{I}2} + p_x^{\mathrm{I}3} - p_x^{\mathrm{I}4}\right)\\ &+ \beta\left(p_y^{\mathrm{R}1} - p_y^{\mathrm{R}2} + p_y^{\mathrm{R}3} - p_y^{\mathrm{R}4}\right)\\ &+ \gamma\left(p_z^{\mathrm{I}1} - p_z^{\mathrm{I}2} - p_z^{\mathrm{I}3} + p_z^{\mathrm{I}4}\right)\\ &+ \gamma'\left(p_z^{\mathrm{R}1} - p_z^{\mathrm{R}2} - p_z^{\mathrm{R}3} + p_z^{\mathrm{R}4}\right),\end{aligned} \tag{B1}$$

$$\begin{aligned}\left|\Psi^v_{\mathrm{mol}}\right\rangle \propto\ & \alpha'\left(p_x^{\mathrm{I}1} + p_x^{\mathrm{I}2} + p_x^{\mathrm{I}3} + p_x^{\mathrm{I}4}\right)\\ &+ \alpha''\left(p_x^{\mathrm{R}1} + p_x^{\mathrm{R}2} + p_x^{\mathrm{R}3} + p_x^{\mathrm{R}4}\right)\\ &\times \gamma''\left(p_z^{\mathrm{I}1} + p_z^{\mathrm{I}2} - p_z^{\mathrm{I}3} - p_z^{\mathrm{I}4}\right).\end{aligned} \tag{B2}$$

As can be seen the eigenvalues of $(\tilde{C}_{2x}, \tilde{C}_{2y}, \tilde{I})$ imply that the p_y orbitals are absent in the valence band states. This is in agreement with Ref. [38]. This reference further suggests that the coefficient β of the p_y orbitals in the conduction band is also negligible. The coefficients cannot be fixed by the symmetry argument. But this is already enough to let us construct the most general Hamiltonian compatible with the above eigenvalues. We have used the subscript mol to emphasize the molecular orbital nature of degrees of freedom involved in the low-energy effective theory of borophene. This should be contrasted to a graphene sheet, where atomic p_z orbitals form the low-energy electronic degrees of freedom.

Equations (B1) and (B2) allow us to construct the matrix representation of the generators (and hence all other members) of the $8Pmmn$ group. Let $\tau_i, i = 1, 2, 3$ denote the Pauli matrices acting on the space of the above molecular orbitals. τ_0 is the unit 2×2 matrix. Adding the spin structure, let σ_i denote the Pauli matrices in the space of $\uparrow$ and $\downarrow$ states. Again, σ_0 will be the unit matrix in this space. In this basis, we have the following representation:

$$\tilde{C}_{2x} = i\sigma_1\tau_0, \quad \tilde{C}_{2y} = i\sigma_2\tau_3, \quad \tilde{I} = \sigma_0\tau_3, T = i\sigma_2\tau_0 K, \quad \text{(B3)}$$

where a tenser product $\otimes$ is understood. T is the time reversal and K is the complex conjugation. This representation is on the space of four states $|\Psi^c_{\rm mol}, \pm\frac{1}{2}\rangle$ and $|\Psi^v_{\rm mol}, \pm\frac{1}{2}\rangle$. In this space, the most general 4×4 Hamiltonian can be written as

$$H = d_0(k)\mathbb{1} + \sum_i d_i(k)\Gamma_i + \sum_{ij} d_{ij}(k)\Gamma_{ij}, \quad \text{(B4)}$$

where $\mathbb{1}$ denotes the 4×4 identity matrix and the Γs are suitable basis in the space of 4×4 matrices. One possible explicit representation is given by [67]

$$\begin{aligned}
&\Gamma_1 = \sigma_x \otimes \tau_x, \quad \Gamma_2 = \sigma_y \otimes \tau_x,\\
&\Gamma_3 = \sigma_z \otimes \tau_x, \quad \Gamma_4 = 1 \otimes \tau_y, \quad \Gamma_5 = 1 \otimes \tau_z,\\
&\Gamma_{ij} = [\sigma_i \otimes \tau_x, \sigma_j \otimes \tau_x]/2i = \epsilon_{ijk}\sigma_k \otimes 1,\\
&\Gamma_{i4} = [\sigma_i \otimes \tau_x, 1 \otimes \tau_y]/2i = \sigma_i \otimes \tau_3,\\
&\Gamma_{i5} = [\sigma_i \otimes \tau_x, 1 \otimes \tau_z]/2i = -\sigma_i \otimes \tau_y,\\
&\Gamma_{45} = [1 \otimes \tau_y, 1 \otimes \tau_z]/2i = 1 \otimes \tau_x.
\end{aligned} \quad \text{(B5)}$$

Functions $d_0(k)$, $d_i(k)$ and $d_{ij}(k)$ are polynomials in k. Now using Eq. (B3), one can construct the effect of all symmetry operators g of the $8Pmmn$ group on the above set of Γ matrices by $g : \Gamma \to g\Gamma g^{-1}$.

The properties of Γ matrices under the generators of $8Pmmn$ group operators and time reversal symmetry operator T are given in the following. For $\tilde{C}_{2x}$, we have

$$\begin{aligned}
&\tilde{C}_{2x}\Gamma_1\tilde{C}_{2x} = \Gamma_1, \quad \tilde{C}_{2x}\Gamma_2\tilde{C}_{2x} = -\Gamma_2, \quad \tilde{C}_{2x}\Gamma_3\tilde{C}_{2x} = -\Gamma_3,\\
&\tilde{C}_{2x}\Gamma_4\tilde{C}_{2x} = \Gamma_4, \quad \tilde{C}_{2x}\Gamma_5\tilde{C}_{2x} = \Gamma_5, \quad \tilde{C}_{2x}\Gamma_{45}\tilde{C}_{2x} = \Gamma_{45},\\
&\tilde{C}_{2x}\Gamma_{15}\tilde{C}_{2x} = \Gamma_{15}, \quad \tilde{C}_{2x}\Gamma_{25}\tilde{C}_{2x} = -\Gamma_{25}, \quad \tilde{C}_{2x}\Gamma_{35}\tilde{C}_{2x} = -\Gamma_{35},\\
&\tilde{C}_{2x}\Gamma_{14}\tilde{C}_{2x} = \Gamma_{14}, \quad \tilde{C}_{2x}\Gamma_{24}\tilde{C}_{2x} = -\Gamma_{24}, \quad \tilde{C}_{2x}\Gamma_{34}\tilde{C}_{2x} = -\Gamma_{34},\\
&\tilde{C}_{2x}\Gamma_{12}\tilde{C}_{2x} = -\Gamma_{12}, \quad \tilde{C}_{2x}\Gamma_{13}\tilde{C}_{2x} = -\Gamma_{13}, \quad \tilde{C}_{2x}\Gamma_{23}\tilde{C}_{2x} = \Gamma_{23}.
\end{aligned} \quad \text{(B6)}$$

For $\tilde{C}_{2y}$, we obtain

$$\begin{aligned}
&\tilde{C}_{2y}\Gamma_1\tilde{C}_{2y} = \Gamma_1, \quad \tilde{C}_{2y}\Gamma_2\tilde{C}_{2y} = -\Gamma_2, \quad \tilde{C}_{2y}\Gamma_3\tilde{C}_{2y} = \Gamma_3,\\
&\tilde{C}_{2y}\Gamma_4\tilde{C}_{2y} = -\Gamma_4, \quad \tilde{C}_{2y}\Gamma_5\tilde{C}_{2y} = \Gamma_5, \quad \tilde{C}_{2y}\Gamma_{45}\tilde{C}_{2y} = -\Gamma_{45},\\
&\tilde{C}_{2y}\Gamma_{15}\tilde{C}_{2y} = \Gamma_{15}, \quad \tilde{C}_{2y}\Gamma_{25}\tilde{C}_{2y} = -\Gamma_{25}, \quad \tilde{C}_{2y}\Gamma_{35}\tilde{C}_{2y} = \Gamma_{35},\\
&\tilde{C}_{2y}\Gamma_{14}\tilde{C}_{2y} = -\Gamma_{14}, \quad \tilde{C}_{2y}\Gamma_{24}\tilde{C}_{2y} = \Gamma_{24}, \quad \tilde{C}_{2y}\Gamma_{34}\tilde{C}_{2y} = -\Gamma_{34},\\
&\tilde{C}_{2y}\Gamma_{12}\tilde{C}_{2y} = -\Gamma_{12}, \quad \tilde{C}_{2y}\Gamma_{13}\tilde{C}_{2y} = \Gamma_{13}, \quad \tilde{C}_{2y}\Gamma_{23}\tilde{C}_{2y} = -\Gamma_{23},
\end{aligned} \quad \text{(B7)}$$

Under inversion, they behave as

$$\begin{aligned}
&\tilde{I}\Gamma_1\tilde{I} = -\Gamma_1, \quad \tilde{I}\Gamma_2\tilde{I} = -\Gamma_2, \quad \tilde{I}\Gamma_3\tilde{I} = -\Gamma_3,\\
&\tilde{I}\Gamma_4\tilde{I} = -\Gamma_4, \quad \tilde{I}\Gamma_5\tilde{I} = \Gamma_5, \quad \tilde{I}\Gamma_{45}\tilde{I} = -\Gamma_{45},\\
&\tilde{I}\Gamma_{15}\tilde{I} = -\Gamma_{15}, \quad \tilde{I}\Gamma_{25}\tilde{I} = -\Gamma_{25}, \quad \tilde{I}\Gamma_{35}\tilde{I} = -\Gamma_{35},\\
&\tilde{I}\Gamma_{14}\tilde{I} = \Gamma_{14}, \quad \tilde{I}\Gamma_{24}\tilde{I} = \Gamma_{24}, \quad \tilde{I}\Gamma_{34}\tilde{I} = \Gamma_{34},\\
&\tilde{I}\Gamma_{12}\tilde{I} = \Gamma_{12}, \quad \tilde{I}\Gamma_{13}\tilde{I} = \Gamma_{13}, \quad \tilde{I}\Gamma_{23}\tilde{I} = \Gamma_{23}.
\end{aligned} \quad \text{(B8)}$$

Finally, under time reversal they are transformed as

$$\begin{aligned}
&T\Gamma_i T^{-1} = -\Gamma_i, \quad i = 1, 2, 3, 4,\\
&T\Gamma_5 T^{-1} = \Gamma_5, \quad T\Gamma_{ij}T^{-1} = -\Gamma_{ij} \quad T\Gamma_{i4}T^{-1} = -\Gamma_{i4},\\
&T\Gamma_{i5}T^{-1} = \Gamma_{i5} \quad i.j = 1, 2, 3,\\
&T\Gamma_{45}T^{-1} = \Gamma_{45}.
\end{aligned} \quad \text{(B9)}$$

Then using the character Table I the Γ matrices can be classified in terms of the irreducible representations. We have summarized the result of this procedure in Table II.

The middle column denotes the irreducible representations of the $8Pmmn$ group. It turns out that all the 16 Γ-matrices belong to one-dimensional representations of the $8Pmmn$ group. These are denoted in the right column, along with their signature under TR operation. Corresponding basis functions up to third-order polynomials along with their signature under TR are given in the left column. Since none of the matrices belongs to B_{1g} representation, the corresponding entry is empty. In A_u and B_{1u}, representations in rows number 10 and 11, the basis functions can only have "+" signature under the TR. So, there is no basis function with "−" TR signature to couple to Γ_1 and Γ_2 matrices. Similarly, in B_{2u} and B_{3u}, irreducible representations of the last two rows, the basis functions are odd under TR, and there is no TR-even basis function to couple to Γ_{35} and Γ_{45} matrices. Now it is straightforward to construct invariant Hamiltonian: Simply multiply basis

TABLE II. Basis functions (polynomials up to third order) and Γ matrices transforming in every irreducible representation. The values of $T = \pm$ denotes the signature under time reversal operation. As for the B field itself, $T = -$ indicates that the TR operates on the whole world.

(Basis; T)	Representation	(Γ matrices; T)
$\{1, k_x^2, k_y^2; +\}$	A_g	$\{\mathrm{I},\ \Gamma_5; +\}$
$\{k_x k_y z; +\}$	A_u	$\{\Gamma_{15}; +\}$
$\{k_x k_y; +\}$	B_{1g}	——
$\{B_z; -\}$	B_{1g}	$\{\Gamma_{12}, \Gamma_{34}; -\}$
$\{z; +\}$	B_{1u}	$\{\Gamma_{25}; +\}$
$\{B_y, zk_x; -\}$	B_{2g}	$\{\Gamma_{13}, \Gamma_{24}; -\}$
$\{k_y, k_x^2 k_y, k_y^3, z^2 k_y; -\}$	B_{2u}	$\{\Gamma_3; -\}$
$\{B_x, zk_y; -\}$	B_{3g}	$\{\Gamma_{14}, \Gamma_{23}; -\}$
$\{k_x, k_x k_y^2, k_x^3, z^2 k_x; -\}$	B_{3u}	$\{\Gamma_4; -\}$
——	A_u	$\{\Gamma_1; -\}$
——	B_{1u}	$\{\Gamma_2; -\}$
——	B_{2u}	$\{\Gamma_{35}; +\}$
——	B_{3u}	$\{\Gamma_{45}; +\}$

functions from the left column in their corresponding matrices in the right column.

Therefore, the most generic $8Pmmn$-invariant 4×4 Hamiltonian $|\psi^c,\frac{1}{2}\rangle$, $|\psi^v,\frac{1}{2}\rangle$, $|\psi^c,-\frac{1}{2}\rangle$, $|\psi^v,-\frac{1}{2}\rangle$ basis is given by

$$\begin{aligned} H &= f(\vec{k})\sigma_0\tau_0 + m(\vec{k})\sigma_0\tau_3 + t_0k_x\sigma_0\tau_2 + \Delta_{\mathrm{KM}}k_y\sigma_3\tau_1 \\ &\quad + \sum_{i,j=1}^{2} k_i\sigma_j\epsilon_{ij}\left(\lambda^R_{0,i}\tau_0 + \lambda^R_{3,i}\tau_3\right) + (\lambda_2\sigma_2 + \lambda_1k_xk_y\sigma_1)\tau_2 \\ &\quad + \sum_{i=1}^{3} B_i\sigma_i g_{0,i}\tau_0 + M_i^{\mathrm{int}}g_{3,i}\tau_3, \end{aligned} \tag{B10}$$

where $f(\vec{k}) = f_0 + f_1k_x^2 + f_2k_y^2$, $m(\vec{k}) = m_1k_x^2 + m_2k_y^2 - m_0$ and we have used the explicit form of Γ matrices in terms of direct product of σ and τ matrices. Δ_{KM} is spin-orbit coupling of the Kane-Mele type [40], $\lambda^R_{0,i}$ and $\lambda^R_{3,i}$ for $i=1,2$ are anisotropic Rashba spin-orbit coupling. $\lambda^R_{0,i}$ is proportional to external electric field [41] while $\lambda^R_{3,i}$ is similar to "buckling" term [28]. λ_1,λ_2 are forms of spin-orbit coupling which are specific to the $8Pmmn$ structure. All λ couplings are proportional to the coordinate z itself, signifying that they are related to a linear potential profile. Those appearing along with τ_3 are "staggered" fields, while those evenly coupled to orbital degrees of freedom are "uniform" fields which can be extrinsically applied. Similarly, in the last line, we have two types of Zeeman coupling. The terms proportional to τ_0 are related to coupling to external field B_i, and the term proportional to τ_3 is due to internal exchange fields which root in the orbital angular momentum of the molecular orbitals involved. In both electric- and magnetic-field-related terms, those couplings carrying index 3 which are coupled to τ_3 arise from internal fields specific to $8Pmmn$ structure. The lack of symmetry under $z\to -z$ prevents them from vanishing.

[1] K. S. Novoselov, A. K. Geim, S. Morozov, D. Jiang, M. Katsnelson, I. Grigorieva, S. Dubonos, and A. A. Firsov, Nature **438**, 197 (2005).

[2] M. I. Katsnelson and M. I. Katsnelson, *Graphene: Carbon in Two Dimensions* (Cambridge University Press, United Kingdom, 2012).

[3] N. P. Armitage, E. J. Mele, and A. Vishwanath, Rev. Mod. Phys. **90**, 015001 (2018).

[4] T. Wehling, A. M. Black-Schaffer, and A. V. Balatsky, Adv. Phys. **63**, 1 (2014).

[5] M. S. Dresselhaus, G. Dresselhaus, and A. Jorio, *Group Theory: Application to the Physics of Condensed Matter* (Springer Science & Business Media, Berlin, Heidelberg, Germany, 2007).

[6] M. D. Schwartz, *Quantum Field Theory and the Standard Model* (Cambridge University Press, United Kingdom, 2014).

[7] M. E. Peskin, *An Introduction to Quantum Field Theory* (CRC Press, Boca Raton, Florida, USA, 2018).

[8] S. A. Jafari, arXiv:1904.01328.

[9] D. C. Cabra, N. E. Grandi, G. A. Silva, and M. B. Sturla, Phys. Rev. B **88**, 045126 (2013).

[10] Y. Mao, W. L. Wang, D. Wei, E. Kaxiras, and J. G. Sodroski, ACS Nano **5**, 1395 (2011).

[11] X. Fan, D. Ma, B. Fu, C.-C. Liu, and Y. Yao, Phys. Rev. B **98**, 195437 (2018).

[12] T. Morinari, T. Himura, and T. Tohyama, J. Phys. Soc. Jpn. **78**, 023704 (2009).

[13] Z. Jalali-Mola and S. A. Jafari, Phys. Rev. B **98**, 195415 (2018).

[14] Z. Jalali-Mola and S. A. Jafari, Phys. Rev. B **98**, 235430 (2018).

[15] K. Kajita, Y. Nishio, N. Tajima, Y. Suzumura, and A. Kobayashi, J. Phys. Soc. Jpn. **83**, 072002 (2014).

[16] J. Nissinen and G. E. Volovik, JETP Lett. **105**, 447 (2017).

[17] G. E. Volovik, JETP Lett. **104**, 645 (2016).

[18] G. E. Volovik, Phys. Usp. **61**, 89 (2018).

[19] S. Carroll, *Spacetime and Geometry: An Introduction to General Relativity* (Pearson, London, England, 2003).

[20] K. Martel and E. Poisson, Am. J. Phys. **69**, 476 (2001).

[21] E. Curiel, Nat. Astron. **3**, 27 (2019).

[22] M. Novello, M. Visser, and G. E. Volovik, *Artificial Black Holes* (World Scientific, Singapore, 2002).

[23] J. Macher and R. Parentani, Phys. Rev. A **80**, 043601 (2009).

[24] J. B. Curtis, G. Refael, and V. Galitski, arXiv:1801.01607.

[25] S. Guan, Z.-M. Yu, Y. Liu, G.-B. Liu, L. Dong, Y. Lu, Y. Yao, and S. A. Yang, npj Quantum Mater. **2**, 23 (2017).

[26] H. Huang, K.-H. Jin, and F. Liu, Phys. Rev. B **98**, 121110(R) (2018).

[27] H. Liu, J.-T. Sun, and S. Meng, Phys. Rev. B **99**, 075121 (2019).

[28] M. Ezawa, Phys. Rev. B **96**, 035425 (2017).

[29] A. J. Mannix, X.-F. Zhou, B. Kiraly, J. D. Wood, D. Alducin, B. D. Myers, X. Liu, B. L. Fisher, U. Santiago, J. R. Guest, M. J. Yacaman, A. Ponce, A. R. Oganov, M. C. Hersam, and N. P. Guisinger, Science **350**, 1513 (2015).

[30] Q. Zhong, J. Zhang, P. Cheng, B. Feng, W. Li, S. Sheng, H. Li, S. Meng, L. Chen, and K. Wu, J. Phys.: Condens. Matter **29**, 095002 (2017).

[31] Q. Zhong, L. Kong, J. Gou, W. Li, S. Sheng, S. Yang, P. Cheng, H. Li, K. Wu, and L. Chen, Phys. Rev. Materials **1**, 021001 (2017).

[32] B. Feng, J. Zhang, Q. Zhong, W. Li, S. Li, H. Li, P. Cheng, S. Meng, L. Chen, and K. Wu, Nat. Chem. **8**, 563 (2016).

[33] Z. Zhang, E. S. Penev, and B. I. Yakobson, Nat. Chem. **8**, 525 (2016).

[34] Z. Zhang, A. J. Mannix, Z. Hu, B. Kiraly, N. P. Guisinger, M. C. Hersam, and B. I. Yakobson, Nano Lett. **16**, 6622 (2016).

[35] H. Tang and S. Ismail-Beigi, Phys. Rev. Lett. **99**, 115501 (2007).

[36] H. Tang and S. Ismail-Beigi, Phys. Rev. B **82**, 115412 (2010).

[37] X.-F. Zhou, X. Dong, A. R. Oganov, Q. Zhu, Y. Tian, and H.-T. Wang, Phys. Rev. Lett. **112**, 085502 (2014).

[38] A. Lopez-Bezanilla and P. B. Littlewood, Phys. Rev. B **93**, 241405(R) (2016).

[39] A. D. Zabolotskiy and Y. E. Lozovik, Phys. Rev. B **94**, 165403 (2016).

[40] C. L. Kane and E. J. Mele, Phys. Rev. Lett. **95**, 226801 (2005).

[41] H. Min, J. E. Hill, N. A. Sinitsyn, B. R. Sahu, L. Kleinman, and A. H. MacDonald, Phys. Rev. B **74**, 165310 (2006).
[42] F. D. M. Haldane, Phys. Rev. Lett. **61**, 2015 (1988).
[43] Y. Tokura, K. Yasuda, and A. Tsukazaki, Nat. Rev. Phys. **1**, 126 (2019).
[44] T. Jungwirth, J. Wunderlich, and K. Olejník, Nat. Mater. **11**, 382 (2012).
[45] A. Manchon, H. C. Koo, J. Nitta, S. M. Frolov, and R. A. Duine, Nat. Mater. **14**, 871 (2015), review article.
[46] J. Balakrishnan, G. K. W. Koon, A. Avsar, Y. Ho, J. H. Lee, M. Jaiswal, S.-J. Baeck, J.-H. Ahn, A. Ferreira, M. A. Cazalilla, A. H. C. Neto, and B. Özyilmaz, Nat. Commun. **5**, 4748 (2014), article .
[47] M. Oliva-Leyva and G. G. Naumis, Phys. Rev. B **88**, 085430 (2013).
[48] J. L. Mañes, F. de Juan, M. Sturla, and M. A. H. Vozmediano, Phys. Rev. B **88**, 155405 (2013).
[49] A. H. Castro Neto and F. Guinea, Phys. Rev. Lett. **103**, 026804 (2009).
[50] S. M. Young and C. L. Kane, Phys. Rev. Lett. **115**, 126803 (2015).
[51] R. Resta, J. Phys.: Condens. Matter **14**, R625 (2002).
[52] R. D. King-Smith and D. Vanderbilt, Phys. Rev. B **47**, 1651 (1993).
[53] Z. Xie, S. He, C. Chen, Y. Feng, H. Yi, A. Liang, L. Zhao, D. Mou, J. He, Y. Peng, X. Liu, Y. Liu, G. Liu, X. Dong, L. Yu, J. Zhang, S. Zhang, Z. Wang, F. Zhang, F. Yang, Q. Peng, X. Wang, C. Chen, Z. Xu, and X. J. Zhou, Nat. Commun. **5**, 3382 (2014), article .
[54] D. Li, B. Rosenstein, B. Y. Shapiro, and I. Shapiro, Phys. Rev. B **95**, 094513 (2017).
[55] M. Ezawa, Phys. Rev. Lett. **109**, 055502 (2012).
[56] M. Bañados, C. Teitelboim, and J. Zanelli, Phys. Rev. Lett. **69**, 1849 (1992).
[57] L. Ryder, *Introduction to General Relativity* (Cambridge University Press, Cambridge, United Kingdom, 2009).
[58] S. Carrol, *Spacetime and Geometry: An Introduction to General Relativity* (Pearson, London, England, 2003).
[59] J. Balakrishnan, G. K. W. Koon, M. Jaiswal, A. C. Neto, and B. Özyilmaz, Nat. Phys. **9**, 284 (2013).
[60] C. Bradley and A. Cracknell, *The Mathematical Theory of Symmetry in Solids: Representation Theory for Point Groups and Space Groups* (Oxford University Press, Oxford, England, UK, 2010).
[61] P. R. Bunkar, *Molecular Symmetry and Spectroscopy* (Academic Press, Cambridge, Massachusetts, 1979).
[62] C. Kittel, *Quantum Theory of Solids,* 2nd revised ed. (John Wiley and Sons, New Jersey, 1983).
[63] L. Elcoro, B. Bradlyn, Z. Wang, M. G. Vergniory, J. Cano, C. Felser, B. A. Bernevig, D. Orobengoa, G. Flor, and M. I. Aroyo, J. Appl. Crystallogr. **50**, 1457 (2017).
[64] B. Bradlyn, L. Elcoro, J. Cano, M. Vergniory, Z. Wang, C. Felser, M. Aroyo, and B. A. Bernevig, Nature **547**, 298 (2017).
[65] J. Cano, B. Bradlyn, Z. Wang, L. Elcoro, M. G. Vergniory, C. Felser, M. I. Aroyo, and B. A. Bernevig, Phys. Rev. B **97**, 035139 (2018).
[66] B. Bradlyn, L. Elcoro, M. G. Vergniory, J. Cano, Z. Wang, C. Felser, M. I. Aroyo, and B. A. Bernevig, Phys. Rev. B **97**, 035138 (2018).
[67] C.-X. Liu, X.-L. Qi, H. J. Zhang, X. Dai, Z. Fang, and S.-C. Zhang, Phys. Rev. B **82**, 045122 (2010).